Front. Phys., 2012, 7(1): 131–146
DOI 10.1007/s11467-011-0236-6

REVIEW ARTICLE

Macroscopic superposition states of ultracold bosons in a double-well potential

M. A. Garcia-March[1,2], **D. R. Dounas-Frazer**[3], **Lincoln D. Carr**[1,4,†]

[1] *Department of Physics, Colorado School of Mines, Golden, CO 80401, USA*
[2] *Department of Physics, University College Cork, Cork, Ireland*
[3] *Department of Physics, University of California, Berkeley, CA 94720, USA*
[4] *Universität Heidelberg, Physikalisches Institut, Philosophenweg 12, D-69120 Heidelberg, Germany*
E-mail: †*lcarr@mines.edu*
Received November 8, 2011; accepted December 7, 2012

We present a thorough description of the physical regimes for ultracold bosons in double wells, with special attention paid to macroscopic superpositions (MSs). We use a generalization of the Lipkin–Meshkov–Glick Hamiltonian of up to eight single particle modes to study these MSs, solving the Hamiltonian with a combination of numerical exact diagonalization and high-order perturbation theory. The MS is between left and right potential wells; the extreme case with all atoms simultaneously located in both wells and in only two modes is the famous NOON state, but our approach encompasses much more general MSs. Use of more single particle modes brings dimensionality into the problem, allows us to set hard limits on the use of the original two-mode LMG model commonly treated in the literature, and also introduces a mixed Josephson–Fock regime. Higher modes introduce angular degrees of freedom and MS states with different angular properties.

Keywords macroscopic superposition states, ultracold bosons in double-well potentials

PACS numbers 03.75.Hh, 03.75.Lm, 03.75.Gg, 03.65.Ud

Contents

1 Introduction 131
2 Second quantized Hamiltonian 133
3 One-dimensional Lipkin–Meshkov–Glick Hamiltonian 134
4 Characterization of the eigenstates 135
4.1 General considerations 135
4.2 Non-interacting regime 136
4.3 Fock regime 137
5 Characterization of the bounds of the model, regimes, and crossings 137
5.1 Limits of the two-level model 137
5.2 Discussion of the different regimes 138
5.3 Crossings of the eigenvalues 140
6 Three-dimensional double well 142
7 Conclusions 143
Acknowledgements 144
References 144

1 Introduction

The superposition of quantum states is a postulate in quantum mechanics. When these states can be distinguished macroscopically it leads to the fundamental question of how the theory describing the physics of point particles or atoms is connected with macroscopic objects [1]. Ultracold bosons in double wells provide a useful realization of macroscopic superposition (MS) states, in which the distinguishable macroscopic property is the localization of atoms in one of the wells [2–4]. In this system, it is possible to restrict the atoms to occupy only two single particle modes, corresponding to their being condensed in the lowest energy state and localized spatially in one of the wells [5, 6]. In this simplified two mode picture, the main two processes are the tunneling of atoms between wells and their interaction in pairs in one of the wells. When the tunneling energy is larger than the interaction energy, this is an ideal system for studying Josephson effects [7–21], when interactions

©Higher Education Press and Springer-Verlag Berlin Heidelberg 2012

dominate over tunneling, MSs can be obtained [2, 22–24]. When all N atoms occupy simultaneously the two single particle states localized in each well, these MSs are known as NOON states. The tunneling dominated regime is known as the *Josephson regime*, while the interaction regime is known as the *Fock regime*. In the latter, the two mode approach can cease to be sufficient to describe the system, due to large interactions populating single particle excited states. Here, we offer a detailed study of the eigenvector spectra in one-dimensional (1D) double wells, with special attention to the appearance of MS states which occur in the Fock regime, and we include more modes in our approach, as appropriate for this regime. We also present the extension to the three dimensional (3D) case, which was discussed extensively in Ref. [25], and compare both cases.

To model 1D double wells we use a four-mode generalization of the Lipkin–Meshkov–Glick Hamiltonian (LMGH) [26, 27], where the atoms are allowed to occupy two excited on-well (sometimes called on-site) localized single particle eigenstates [see Fig. 1(a)]. Due to the new two excited modes, there are three new processes in the model. On the one hand, pairs of atoms in the ground state in one well can be excited to the first level, or decay from this level to the ground state, as sketched in Fig. 1(a). Also, the atoms excited to the first level of eigenenergies can interact on-well or tunnel to the other well, also sketched in Fig. 1(a). Then, in this picture, the conventional division into the Josephson and Fock regimes must be amended to include a new *mixed regime,* in which the atoms behave differently depending on their energy level, as discussed in Section 5. We use perturbation theory to characterize the eigenstates and eigenvalues in the Fock regime and we also characterize them analytically in the non-interacting regime. In between these two regimes, we use numerical exact diagonalization of the LMGH to show how the transition between these regimes occurs. We identify clearly the regimes in which the original NOON states as well as novel MS states can be obtained. We characterize the limits of the model, the occurrence of crossings in the spectra, and couplings between states with atoms in different levels. Our crossing criteria clarify when the *one-level approximation* (LMGH with only two modes) ceases to be sufficient, and one must use at least the *two-level approximation.*

The four-mode, two-level generalization of the LMGH is the natural way to introduce dimensionality in the problem. When the same two levels are generalized to 3D double wells, an eight-mode generalization of the LMGH is obtained as sketched in Fig. 1(b). Then, a new quantum number, the orbital degree of freedom, is introduced and it plays a key role [25]. Since new parameters arise in the 3D case, new dynamical regimes are found. Moreover, new MS states involving angular degrees of freedom can

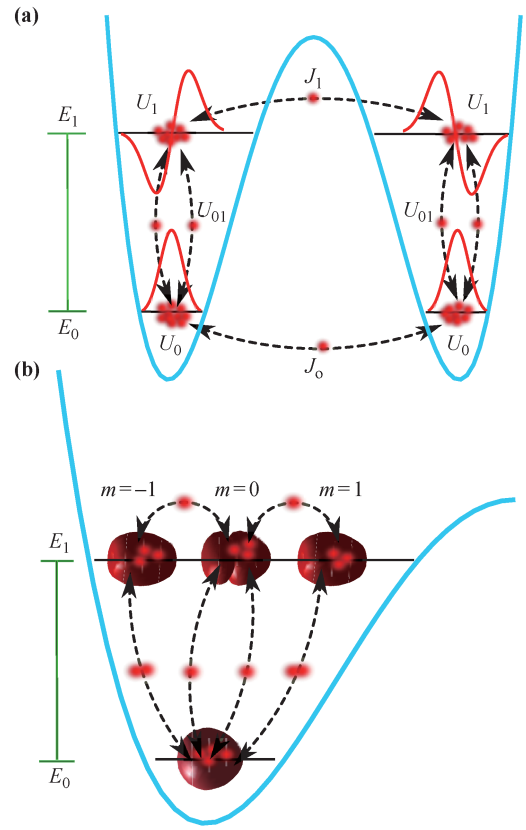

Fig. 1 Schematic of the double well. **(a)** 1D: the J's indicate single-particle tunneling processes while the U's indicate two-particle tunneling and interaction processes. **(b)** 3D: the spherical harmonics $Y_{\ell m}$, with total and z-component of the angular momentum ℓ and m respectively, are distorted by the coupling to the nearby well.

occur. In a previous work we characterized the limits of the one- and two-level approximations, the occurrence of crossings in different regimes, and the coupling between states with atoms in different levels [25]. In this Article we review, complete, and extend the 1D picture obtained in Refs. [2, 28]. We also compare with the 3D case, and summarize the derivation of the 3D two-level LMGH and the routes to new physics in 3D which are currently being explored.

By means of a semiclassical, mean-field approximation macroscopic quantum tunneling has been predicted in the Josephson regime, while macroscopic self-trapping in one of the wells has been shown to occur when the interactions grow [7–18]. The macroscopic quantum tunneling and self-trapping were observed in a recent experiment [19]. The former can be understood as the d.c. Josephson effect for superconductors, while the a.c. Josephson effect corresponds to small oscillations in the difference between the populations in both wells obtained for bigger interactions [20]. The a.c. Josephson effect was recently demonstrated experimentally [21]. One perspective is that the energy levels depend on the occupation of one of the wells. Then one can analyze the double well problem in terms of Landau–Zener tunneling. In this case

the energy between levels changes with a constant small rate, leading to an adiabatically driven Josephson junction [29–31].

In the Fock regime the semiclassical approach ceases to be appropriate, and other approaches can be useful; the most numerically accurate but also the most computationally intensive is the multiconfigurational Hartree method [32–36]. Methods based on the LMGH [26, 27], although limited to weaker interactions, have the advantage that one can treat more particles in higher dimensions, as well as make use of perturbation theory to obtain analytical results [2, 37]. In this Article we use a modified LMGH for these reasons. The LMGH was first introduced in the framework of nuclear physics [26]. It has applications in a wide range of other fields, like ultracold bosons, and it is a perfect simple Hamiltonian to study a vast range of quantum effects, from quantum phase transitions [27, 38] to Josephson oscillations. The LMGH also applies in cold atoms for two hyperfine boson species in a single well, where MS states are predicted to occur [39, 40]. In this Fock regime the two mode approach could be insufficient to characterize the problem, since crossings and coupling to other more excited single particle states may be possible. Indeed, it is necessary to consider a second level in 1D for the physical parameters found in typical BEC experimental systems [2]. To consider this possibility we use a four-mode generalization of the LMGH for 1D double wells and an eight mode characterization in the 3D case.

Besides being a good system for fundamental studies of quantum many body effects, ultracold bosons in double wells also have many technological applications, for example, in quantum high precision measurements of inertial and gravitational fields [41, 42], as a primary thermometer [43], or in quantum computing [44–46].

The Article is organized as follows. In Section 2 we introduce the initial second quantized Hamiltonian. In Section 3 we obtain the 1D four-mode LMGH. Then, in Section 4 we characterize the eigenvectors and eigenvalues in 1D for the Josephson and Fock regimes. In Section 5 we obtain the limits of the model and the occurrence of crossings, we discuss all possible regimes, and we offer numerical examples to illustrate the results. Finally, we derive the 3D Hamiltonian and compare with the 1D case in Section 6. We conclude, summarize, and discuss lines of future research in Section 7.

2 Second quantized Hamiltonian

The second quantized Hamiltonian for N interacting bosons of mass $\mathcal{M}$ confined by an external potential $V(\boldsymbol{x})$ with $\boldsymbol{x} \in \mathbb{R}^3$ in terms of the bosonic creation and annihilation field operators $\hat{\Psi}(\boldsymbol{x})$, $\hat{\Psi}^\dagger(\boldsymbol{x})$, obeying the usual commutation relations, is

$$\hat{H} = \int \mathrm{d}\boldsymbol{x}\, \hat{\Psi}^\dagger(\boldsymbol{x}) \left[-\frac{\hbar^2}{2\mathcal{M}}\nabla^2 + V(\boldsymbol{x})\right] \hat{\Psi}(\boldsymbol{x}) + \frac{1}{2}\int \mathrm{d}\boldsymbol{x}\, \hat{\Psi}^\dagger(\boldsymbol{x}) \left[\int \mathrm{d}\boldsymbol{x}'\, \hat{\Psi}^\dagger(\boldsymbol{x}') V_{\mathrm{int}}(\boldsymbol{x}-\boldsymbol{x}')\, \hat{\Psi}(\boldsymbol{x}')\right] \hat{\Psi}(\boldsymbol{x}) \tag{1}$$

where $V_{\mathrm{int}}(\boldsymbol{x}-\boldsymbol{x}')$ stands for the two-body interaction and $V(\boldsymbol{x})$ is a three dimensional double-well potential with minima at $\boldsymbol{x} = \pm\boldsymbol{a} \in \mathbb{R}^3$ and a local maximum at $\boldsymbol{x} = \boldsymbol{0}$. We assume the potential to be separable $V(\boldsymbol{x}) = V(x) + V(y) + V(z)$, but our results are valid for general forms of the double well. We take the 1D potentials in the x and y directions as isotropic harmonic oscillators, that is, $V_x = \frac{1}{2}\omega_x^2 x^2$ and $V_y = \frac{1}{2}\omega_y^2 y^2$, where both frequencies are of the same order. For simplicity, we consider $\omega_x = \omega_y = \omega_\perp$ in the following. A conventional 1D double well potential $V(z)$ of barrier height V_0 can be approximated near its minima at $z = \pm a$ by

$$V(\tilde{z}) \approx \frac{1}{2}\mathcal{M}\omega^2\tilde{z}^2 \tag{2}$$

where $\tilde{z} = z \pm a$ and

$$\omega \equiv \left(\frac{1}{\mathcal{M}}\frac{\partial^2 V}{\partial z^2}\right)^{1/2}_{z=a} \tag{3}$$

is the local trapping frequency in each well. The recoil energy, defined as $E_r = \hbar^2/(\mathcal{M}a^2)$, is used through the dimensionless parameter V_0/E_r to determine the barrier height in most of the experiments, with $\lambda = 2a$ an effective wavelength.

We consider the same assumptions discussed in Ref. [25], that is, we assume first that ω is of the same order as $\omega_\perp$ and we consider low densities, for which only binary collisions are relevant; also, we consider low energies, when these collisions are characterized by the s-wave scattering length of the atoms, a_s. The diluteness condition for a weakly interacting Bose gas is

$$\sqrt{|\bar{n}\, a_s^3|} \ll 1 \tag{4}$$

where $\bar{n}$ is the average density of the gas. In the context of the double-well potential, the maximum density of the gas is approximately $\bar{n} = N/(\sqrt{2\pi}\, a_{\mathrm{ho}})^3$, where a_{ho} is the harmonic oscillator length given by $a_{\mathrm{ho}} = \sqrt{\hbar/(\mathcal{M}\omega)}$ (a similar condition must hold in the other two directions). Correspondingly, we restrict our discussion to the regime

$$N^{1/3} \ll \left|\sqrt{2\pi}\, a_{\mathrm{ho}}/a_s\right| \tag{5}$$

Although the system is said to be weakly interacting when condition (5) is met, the interaction energy can be on the order of the kinetic energy and dilute gases can therefore exhibit non-ideal behavior [5, 6]. Under

these conditions the second quantized Hamiltonian can be approximated as

$$\hat{H} = \int \mathrm{d}^3\boldsymbol{x}\, \hat{\Psi}^\dagger(\boldsymbol{x}) \left[-\frac{\hbar^2}{2\mathcal{M}}\nabla^2 + V(\boldsymbol{x})\right] \hat{\Psi}(\boldsymbol{x}) + \frac{g}{2}\int \mathrm{d}^3\boldsymbol{x}\, \hat{\Psi}^\dagger(\boldsymbol{x})\hat{\Psi}^\dagger(\boldsymbol{x})\hat{\Psi}(\boldsymbol{x})\hat{\Psi}(\boldsymbol{x}) \tag{6}$$

The coupling constant g is proportional to the s-wave scattering length, $g = 4\pi\hbar^2 a_s/\mathcal{M}$; in Eq. (6) we took the two-body potential from Eq. (1) to be approximated by an effective local interaction $V_{\mathrm{int}}(\boldsymbol{x}-\boldsymbol{x}') = g\,\delta^{(3)}(\boldsymbol{x}-\boldsymbol{x}')$.

3 One-dimensional Lipkin–Meshkov–Glick Hamiltonian

Let us consider first the reduced 1D case, taking $\omega \ll \omega_\perp$. The double-well potential can be reduced to one spatial dimension in extremely anisotropic traps, where the transverse trapping frequencies must be sufficiently high to reduce the dimensionality of the single-particle wavefunctions. However, one must avoid potential resonances by not squeezing the trap too tightly [47]: it is sufficient that the transverse harmonic oscillator length $a_{\mathrm{ho},\perp} \equiv \sqrt{\hbar/(\mathcal{M}\omega_\perp)} \gg a_s$. Under these assumptions, we can reduce the dimensionality of the second quantized Hamiltonian, by considering that the particles interact and tunnel only in one-dimension. Now, the interactions can be modelled by a 1D delta potential $V_{\mathrm{int}}(z-z') = g_{1\mathrm{D}}\,\delta(z-z')$, with 1D coupling constant $g_{1\mathrm{D}} = g/[2\pi a_\perp^2(1-Ca_s/a_\perp)]$, where C is a dimensionless constant [47, 48]. Then, we can use appropriate superpositions of the eigenfunctions of the 1D single particle Hamiltonian

$$H_{\mathrm{sp}} = -\frac{\hbar^2}{2\mathcal{M}}\nabla^2 + V(z) \tag{7}$$

to obtain a set of on-well localized wavefunctions, in an analogous way that on-site Wannier states are obtained from Bloch functions on a lattice [49]. We use this set of functions to expand the field operator:

$$\hat{\Psi}(z) = \sum_{j,l} \hat{b}_{j\ell}\psi_\ell(z-z_j) \tag{8}$$

where $\psi_\ell(z-z_j)$ are the on-well localized functions. Here, $z_L \equiv -a$ and $z_R \equiv a$ are the minima of the left and right wells, respectively, $j \in \{L, R\}$ is the *well index*, and the label ℓ is the *level index*. The level index increases with single particle energies in each well. For the two level approach considered here, $\ell \in \{0, 1\}$. The operators $\hat{b}_{j\ell}$ and $\hat{b}^\dagger_{j\ell}$ satisfy the usual bosonic annihilation and creation commutation relations,

$$[\hat{b}^\dagger_{j\ell}, \hat{b}_{j'\ell'}] = \delta_{jj'}\delta_{\ell\ell'}$$
$$[\hat{b}_{j\ell}, \hat{b}_{j'\ell'}] = [\hat{b}^\dagger_{j\ell}, \hat{b}^\dagger_{j'\ell'}] = 0 \tag{9}$$

Let $\varphi^n(z)$ be the nth eigenfunction of Hamiltonian (7), with eigenvalue ϵ_n. Then, the localized functions at well j are

$$\psi_{j0}(z) = \frac{1}{\sqrt{2}}[\varphi^1(z) \pm \varphi^2(z)] \tag{10}$$

$$\psi_{j1}(z) = \frac{1}{\sqrt{2}}[\varphi^3(z) \pm \varphi^4(z)] \tag{11}$$

with $j = L$ for the plus sign and $j = R$ for the minus sign. The corresponding eigenvalues are $E_0 = (\epsilon^1 + \epsilon^2)/2$ and $E_1 = (\epsilon^3 + \epsilon^4)/2$. These on-well localized eigenfunctions are represented schematically in Fig. 1(a).

Substituting Eq. (8) into the second quantized Hamiltonian (6) yields the two-level Hamiltonian:

$$\hat{H} = \hat{H}_0 + \hat{H}_1 + \hat{H}_{01} \tag{12}$$

with

$$\hat{H}_\ell = -J_\ell \sum_{j\neq j'} \hat{b}^\dagger_{j\ell}\hat{b}_{j'\ell} + U_{\ell\ell}\sum_j \hat{n}_{j\ell}\,(\hat{n}_{j\ell}-1) + E_\ell \sum_j \hat{n}_{j\ell} \tag{13}$$

$$\hat{H}_{01} = U_{01}\sum_{j,\ell\neq\ell'}\left(2\hat{n}_{j\ell}\hat{n}_{j\ell'} + \hat{b}^\dagger_{j\ell}\hat{b}^\dagger_{j\ell}\hat{b}_{j\ell'}\hat{b}_{j\ell'}\right) \tag{14}$$

where $\hat{n}_{j\ell} \equiv \hat{b}^\dagger_{j\ell}\hat{b}_{j\ell}$ is the number operator. The hopping and interaction terms are

$$J_\ell = -\int \mathrm{d}z\psi^*_\ell(z-a)\left[-\frac{\hbar^2}{2\mathcal{M}}\nabla^2 + V(z)\right]\psi_\ell(z+a) \tag{15}$$

and

$$U_{\ell\ell'} = \frac{g_{1\mathrm{D}}}{2}\int \mathrm{d}z|\psi_\ell(z)|^2|\psi_{\ell'}(z)|^2 \tag{16}$$

respectively. In the following, we denote $U_{\ell\ell}$ simply as U_ℓ.

The functions $\psi_\ell(z)$ resemble roughly the eigenfunctions of the harmonic oscillator potential:

$$\psi_0(\tilde{z}) = a_{\mathrm{ho}}^{-1/2}\pi^{-1/4}\mathrm{e}^{-\tilde{z}^2/(2a_{\mathrm{ho}}^2)} \tag{17}$$

$$\psi_1(\tilde{z}) = a_{\mathrm{ho}}^{-1/2}\sqrt{2}\,\pi^{-1/4}(\tilde{z}/a_{\mathrm{ho}})\mathrm{e}^{-\tilde{z}^2/(2a_{\mathrm{ho}}^2)} \tag{18}$$

The energy of an atom associated with the wavefunction $\psi_\ell(\tilde{z} = z - z_j)$ is $E_l \approx \hbar\omega(\ell + 1/2)$. This approximation fails when the overlap between different on-well localized eigenfunctions is small. Then, in general, it gives a poor approximation of the J_ℓ coefficients given in Eq. (15). Nevertheless, they can be used to obtain a good approximation for the overlap integrals purely on-well, like those defining the $U_{\ell\ell'}$ coefficients, Eq. (16). This is valid for both regimes, though it gives only a rough idea of these coefficients when the actual single particle eigenfunctions are highly distorted, as occurs in the Josephson regime. In this case, it can only be used to obtain scaling relations in the problem. By solving these integrals analytically using Eq. (17) to approximate the single particle eigenfunctions, we obtain

$$U_0 = \frac{g_{1\mathrm{D}}}{\sqrt{2\pi}a_{\mathrm{ho}}} \tag{19}$$

Moreover, we can relate the other interaction coefficients to U_0 by solving the corresponding integrals, which gives $U_1 = (3/4)U_0$ and $U_{01} = (1/2)U_0$. Here we use these expressions in the illustrative examples presented in Section 5, though for actual potentials to obtain accurate values for these coefficients, it is necessary to calculate the single particle eigenfunctions numerically to solve the integrals (16).

Finally, to deduce the Hamiltonian (12) we neglected off-site interactions. These correspond to interaction terms like

$$U_{\ell\ell'}^{jj'} = \frac{g_{1\mathrm{D}}}{2}\int \mathrm{d}z|\psi_\ell(z-z_j)|^2|\psi_{\ell'}(z-z_{j'})|^2 \tag{20}$$

where $j \neq j'$. If the barrier is infinitely high these integrals vanish. If the single particle eigenfunctions are approximated by Eq. (18) this integral gives $U_0\exp[-(a/a_{\mathrm{ho}})^2]$. Then, one could assume that these terms can be neglected for sufficiently high or separated wells, that is, if $a_{\mathrm{ho}} \ll a$. Nevertheless, these are not on-well integrals and then the expressions of the harmonic oscillator eigenfunctions, Eq. (18) do not give accurate results. Then these integrals have to be evaluated numerically for the actual potential and for the correct numerically evaluated single particle eigenfunctions. Moreover, these coefficients have to be compared with J_ℓ to justify their being neglected, since both quantities could be comparable in the Fock regime. In the Josephson regime we can safely neglect these coefficients since they are much smaller than any other interaction coefficient, which in turn are smaller than the tunneling ones. For the Fock regime, we assume that the tunneling coefficients are always bigger that these cross-terms, and have verified that our assumption holds for a number of specific cases. We refer the reader to Ref. [50] for a thorough discussion of the effect of these terms.

4 Characterization of the eigenstates

4.1 General considerations

An arbitrary state vector $|\Psi\rangle$, in the solution space of the two-level Hamiltonian Eq. (12), can be expressed in Fock space as

$$|\Psi\rangle = \sum_{i=0}^{\Omega-1} c_i|i\rangle, \quad |i\rangle = \bigotimes_{j,\ell}|n_{j\ell}^{(i)}\rangle \tag{21}$$

where

$$|n_{j\ell}^{(i)}\rangle = \frac{1}{\sqrt{n_{j\ell}!}}\left(\hat{b}_{j\ell}^\dagger\right)^{n_{j\ell}^{(i)}}|0\rangle \tag{22}$$

Here Ω is the dimension of the Hilbert space $\{|i\rangle\}$, i is the *Fock index*, and $|c_i|^2$ is the probability of finding the atoms distributed between different energy levels and wells in the Fock vector $|i\rangle$, when the system is described by state $|\Psi\rangle$, that is $c_i = \langle i|\Psi\rangle$; henceforth we refer to c_i as the *Fock-space amplitude*. The Fock vector $|i\rangle$ can also be written in longer form as

$$|i\rangle = |n_{L0}^{(i)}, n_{R0}^{(i)}\rangle|n_{L1}^{(i)}, n_{R1}^{(i)}\rangle \tag{23}$$

indicating the occupation of each well (L, R) and each level (0,1) associated with Fock index i. We work in the canonical ensemble, i.e., we require the total number of particles

$$N = \sum_{j\ell} n_{j\ell} \tag{24}$$

to be constant.

The Fock index i is chosen to increase starting with the number of atoms in well $j = L$, and then subsequently increasing with the number of atoms in the same, left well moving up into the excited level $\ell = 1$. Therefore, for the first $N+1$ Fock vectors $i = 1+n_{L0}$ and they correspond with vectors with no occupation of the excited level. Then, they satisfy

$$|i\rangle = \frac{1}{\sqrt{n_{L0}!n_{R0}!}}\left(\hat{b}_{L0}^\dagger\right)^{n_{L0}}\left(\hat{b}_{R0}^\dagger\right)^{n_{R0}}|0\rangle \tag{25}$$

for $i = 0,\ 1,\ \cdots,\ N$. For example, for $N = 2$, the Fock vectors with index $i = 1, 2, 3$ are $|0,2\rangle|0,0\rangle$, $|1,1\rangle|0,0\rangle$, and $|2,0\rangle|0,0\rangle$, respectively. The one-level approximation can easily be recovered from Eq. (12) by requiring $i \leqslant N+1$. In this truncated space, the dimension of the Hilbert space reduces to that of the one-level approximation, namely, $N+1$, and the two-level Hamiltonian $\hat{H}$ reduces to the one-level Hamiltonian $\hat{H}_0$.

A general expression for the Fock index is

$$i = 1 + n_{L0} + \sum_{p=-1}^{N_1-1}(N+1-p)(1+p) + (N+1-N_1)n_{L1} \tag{26}$$

where N_1 is the number of atoms in the excited level. Then, the following Fock vectors for $N = 2$ are $|0,1\rangle|0,1\rangle$, $|1,0\rangle|0,1\rangle$, $|0,1\rangle|1,0\rangle$, and $|1,0\rangle|1,0\rangle$ with indices $i = 4, 5, 6, 7$. The last three show occupation only of the excited level and they are $|0,0\rangle|0,2\rangle$, $|0,0\rangle|1,1\rangle$, and $|0,0\rangle|2,0\rangle$, for $i = 8, 9, 10$. Thus for just two atoms there are already 10 states in our two-level problem, and with increasing N it is necessary to use numerical matrix methods to keep track.

The eigenstates $|\phi^{(k)}\rangle$ of the two-level Hamiltonian (12) satisfy

$$\hat{H}|\phi^{(k)}\rangle = \varepsilon^{(k)}|\phi^{(k)}\rangle \tag{27}$$

where $\varepsilon^{(k)}$ is the energy eigenvalue corresponding to the state $|\phi^{(k)}\rangle$. The eigenstate label k is chosen to increase

with $\varepsilon^{(k)}$. In order to describe these states, we will use the previously introduced Fock-space amplitudes

$$c_i^{(k)} = \langle i\,|\phi^{(k)}\rangle \tag{28}$$

now containing two separate indices for clarity: i is the Fock index, describing the ordering of the Fock basis; k is the energy index, describing the ordering of the energy eigenvalues.

When interlevel effects are not relevant, the eigenstates fall into one of two categories: *harmonic-oscillator-like states*, and *macroscopic superposition states* (MS states). When the barrier between wells is low, $J_0 \gg NU_0$, all states are harmonic oscillator-like (HO) states. This is the Josephson regime and it is characterized by

$$\xi_{J_\ell} = N/\zeta_\ell \ll 1 \tag{29}$$

where $\zeta_\ell = J_\ell/U_\ell$. This criterion must be evaluated separately for both levels, since $J_1 > J_0$, while the interaction terms are of the same order.

On the other hand, MS states dominate the spectrum in the high barrier limit. This is the Fock regime, in which

$$\xi_{U_\ell} = \zeta_\ell \ll 1 \tag{30}$$

Again, this criterion must be evaluated separately for the two levels.

When the level spacing is comparable to NU_0, interlevel effects can no longer be neglected, and a third category of eigenstates emerges. These states show weak coupling between states with particles only in the lowest energy level and others with particles in the excited one. We name these coupled excited states *shadows of the MS states*, because in a surface plot of the Fock-space amplitudes as a function of both energy and Fock index, they appear as faint copies of the MS states with occupation only of the lower level at higher Fock index [25]. In the following two subsections we characterize the eigenstates in the Josephson and Fock regimes.

4.2 Non-interacting regime

Let us consider the extreme Josephson regime, or non-interacting regime, for which $U_\ell = 0$. The Hamiltonian reduces to $\hat{H} = \hat{H}_0 + \hat{H}_1$, with

$$\hat{H}_\ell = -J_\ell \sum_{j\neq j'} \hat{b}_j^{\ell\dagger}\hat{b}_{j'}^{\ell} + E_\ell \sum_j \hat{n}_{j\ell} \tag{31}$$

Since the Hamiltonian is clearly separable, its eigenstates $|\phi^{(k)}\rangle$ are a direct product of the one-level ones, $|\phi^{(K_\ell^{(k)})}\rangle$:

$$|\phi^{(k)}\rangle = \bigotimes_\ell |\phi^{(K_\ell^{(k)})}\rangle \tag{32}$$

where $K_\ell^{(k)} = 0, 1, \cdots, N_\ell^{(k)}$ is the one-level eigenstate label and for the kth eigenstate there are $N_\ell^{(k)}$ atoms at level ℓ. Since the total number of atoms is conserved, $\sum_{\ell=0,1} N_\ell^{(k)} = N$. The one-level eigenstates can be expressed as $|\phi^{(K_\ell^{(k)})}\rangle = \sum c_{i\ell}^{(k)}|n_{L\ell}^{(k)}, n_{R\ell}^{(k)}\rangle$ with

$$c_{i\ell}^{(k)} = a_{K_\ell^{(k)}}(N_\ell^{(k)})h_{K_\ell^{(k)}}(n_{L\ell}^{(k)}|N_\ell^{(k)})p(n_{L\ell}^{(k)}|N_\ell^{(k)}) \tag{33}$$

where $n_{L\ell}^{(k)}$ is the occupation of the left well for the corresponding Fock vector, $h_{K_\ell^{(k)}}(n_{L\ell}^{(k)}|N_\ell^{(k)})$ is a $K_\ell^{(k)}$-th order discrete Hermite polynomial, $p(n_{L\ell}^{(k)}|N_\ell^{(k)})$ is the square root of the binomial distribution,

$$p\left(n_{L\ell}^{(k)}\,\middle|\,N_\ell^{(k)}\right) = \frac{1}{2^{N_\ell^{(k)}/2}}\sqrt{\frac{N_\ell^{(k)}!}{n_{L\ell}!(N_\ell^{(k)}-n_{L\ell}^{(k)})!}} \tag{34}$$

and $a_{K_\ell^{(k)}}(N_\ell^{(k)})$ is the normalization factor

$$a_{K_\ell^{(k)}}(N_\ell^{(k)}) = \sqrt{\frac{(N_\ell^{(k)}-K_\ell^{(k)})!}{N_\ell^{(k)}!\,K_\ell^{(k)}!}} \tag{35}$$

The eigenenergies $\varepsilon^{(k)}$ can be expressed in terms of the one-level eigenenergies as

$$\varepsilon^{(k)} = \sum_\ell \varepsilon_{(k)\ell} \tag{36}$$

where

$$\varepsilon_{(k),\ell} = -J_\ell\left(N_\ell^{(k)} - 2K_\ell^{(k)}\right) + E_\ell N_\ell^{(k)} \tag{37}$$

The one-level Hamiltonian, expressed in the Fock basis is, in the non-interacting limit, a harmonic oscillator potential truncated at hard walls. The analytical expressions of the Fock-space amplitudes $c_{i\ell}^{(k)}$ resemble the probability amplitudes of observing the particle in position x for the 1D harmonic oscillator problem, obtained from the expression of its eigenfunctions in the position representation. Moreover, in both cases the eigenvalues $\varepsilon_{k\ell}$ are linear in $K_\ell^{(k)}$. The analogy can be established between occupation of the wells in the double well and the positions in the Harmonic oscillator problem. Since one variable is discrete while the other is continuous the analogy is valid for the limit of infinite particles. Let us show this for the one level approach, which we obtain considering $\hat{H} = \hat{H}_0$, where $\hat{H}_0$ is given by Eq. (31). In the Heisenberg picture the evolution of the operators $\hat{b}_{j0}$ for $j = L, R$ is given by

$$\mathrm{i}\frac{\mathrm{d}\hat{b}_{j0}}{\mathrm{d}t} = [\hat{b}_{j0}, \hat{H}] = -J\hat{b}_{j'0} \tag{38}$$

with $j' \neq j$, and where we considered $E_0 = 0$ for simplicity. In the following we omit the level index ℓ because we are considering only the one level approximation. For $N \to \infty$, we can approach the operators by c-numbers $\alpha_j = \sqrt{N_j}\mathrm{e}^{\mathrm{i}\theta_j}$. Substituting we obtain the two corresponding equations of motion which in turn can be obtained from the pendulum Hamiltonian

$$\mathcal{H} = -2J\sqrt{N_L\,N_R}\cos(\theta_L-\theta_R) = -J\,N\sqrt{1-z^2}\cos\theta \tag{39}$$

where $N = N_L+N_R$, $z = (N_L-N_R)/N$, $\theta = \theta_L-\theta_R$. The previous approach is widely known to be extended to the small interacting regime, where it gives a Hamiltonian analogous to that of a non-rigid pendulum. The study of the dynamics of such a Hamiltonian permits one to predict macroscopic quantum tunneling and self-trapping within the semiclassical approach [7–9]. In our case, this can be extended to a harmonic oscillator Hamiltonian, where the angular variables can take any value. The analogy here is with the harmonic oscillator truncated at hard walls, because the number of particles is finite. Due to this analogy, the eigenstates (32) are said to be harmonic-oscillator-like. In Section 5 we obtain numerically the eigenvectors and eigenvalues for small interactions, showing that for non-zero interactions the eigenvectors and eigenvalues closely resemble the ones characterized for the non-interacting regime.

4.3 Fock regime

In the extreme Fock regime, or the infinite-barrier limit, $J_0 = J_1 = 0$. In this regime, the coefficient U_{01} cannot be neglected. Then, the eigenvectors of Hamiltonian (12) are Fock vectors, if we further assume that $2\triangle E \gg N^2U_0$. The latter assumption is needed because the term $\hat{b}^\dagger_{jl}\hat{b}^\dagger_{jl}\hat{b}_{jl'}\hat{b}_{jl'}$ couples Fock vectors with atoms in different levels. As demonstrated in Section 5, this coupling is small under that assumption. In this limit, the eigenvalues are

$$\varepsilon^{(k)} = \sum_\ell \left\{ E_\ell N_\ell^{(k)} + U_\ell\left[2\left(n_{L\ell}^{(k)} - \frac{N_\ell^{(k)}}{2}\right)^2 + N_\ell^{(k)}\left(\frac{N_\ell^{(k)}}{2}-1\right)\right]\right\} + U_{01}\sum_{j\ell} 2\,n_{j\ell}^{(k)}n_{j\ell'}^{(k)} \tag{40}$$

Here, the spectra reflects the main symmetry in the problem: that of discrete rotations of an angle π around an axis perpendicular to the x–y plane that intersects this plane in the origin. This in turn means that the eigenstates, which are the Fock vectors $|n_{L0}, n_{R0}\rangle|n_{L1}, n_{R1}\rangle$, are degenerate in pairs with those obtained for $L \to R$. Small but non-negligible hopping terms, $J_0 \ll U_0$ and $J_1 \ll U_0$, break this degeneracy, as can be shown by non-degenerate high-order perturbation theory. Then, in the small tunneling limit, that is, in the Fock regime, the eigenvectors are quasi-degenerate symmetric and antisymmetric superpositions of those pairs of Fock vectors that are degenerate in the infinite barrier case. For the particular cases in which all atoms occupy the same level the eigenstates are direct products of one-level vectors $|\phi_\ell^\pm\rangle|0,0\rangle_{\ell'}$ with

$$|\phi_\ell^\pm\rangle \equiv \frac{\mathrm{e}^{\mathrm{i}\theta_0}}{\sqrt{2}}\left[\frac{1}{\sqrt{\nu!(N-\nu)!}}\left(\hat{b}^\dagger_{L\ell}\right)^\nu\left(\hat{b}^\dagger_{R\ell}\right)^{N-\nu} \pm \frac{1}{\sqrt{\nu!(N-\nu)!}}\left(\hat{b}^\dagger_{L\ell}\right)^{N-\nu}\left(\hat{b}^\dagger_{R\ell}\right)^\nu\right]|0\rangle \tag{41}$$

for $0 \leqslant \nu < N/2$. These are MS states in which ν and $N-\nu$ atoms simultaneously occupy the ℓ-th energy level of both wells; although the expression might appear complicated, in fact it is just a two-state approximation. We have neglected terms on the order of $(J_\ell/U_\ell)^{N-2\nu}$ and smaller. Here θ_0 is the usual arbitrary phase associated with vectors in a Hilbert space. We will set $\theta_0 = 0$ for the rest of this article.

The special case $\nu = 0$ represents an extreme MS state, or *NOON state*, in which all N atoms simultaneously occupy the left and right wells, which can be written also as $(1/\sqrt{2})\,(|N,0\rangle|0,0\rangle \pm |0,N\rangle|0,0\rangle)$. These symmetric (+) or antisymmetric (−) MS states are nearly degenerate, with a splitting $\Delta\varepsilon_\ell(\nu)$ between the states $|\phi_\ell^+\rangle$ and $|\phi_\ell^-\rangle$ given by

$$\Delta\varepsilon_\ell(\nu) = \frac{4U_\ell[J_\ell/(2U_\ell)]^{N-2\nu}(N-\nu)!}{\nu![(N-2\nu-1)!]^2} \tag{42}$$

up to $(N-2\nu)$-th order in J_ℓ/U_ℓ. General MS states are symmetric/antisymmetric superpositions of Fock vectors with atoms in both levels, that is, $|\nu, N_0-\nu\rangle|\nu', N_1-\nu'\rangle$ and $|N_0-\nu,\nu\rangle|N_1-\nu',\nu'\rangle$, with splittings that are proportional to $(J_0/U_0)^{N_0-2\nu}\,(J_1/U_1)^{N_1-2\nu'}$.

Since $J_1 > J_0$, it is also possible that $J_0 \ll U_0$ but $J_1 > U_0$; this is the mixed regime. The atoms in the lower level behave as in the Josephson regime while the ones in the excited level behave as in the Fock regime. We will show numerical examples of the mixed regime in the following section.

5 Characterization of the bounds of the model, regimes, and crossings

5.1 Limits of the two-level model

Let us find criteria in terms of the characteristic parameters of the problem to describe the limits of all regimes, the occurrence of shadows of the MS states, crossings, and the limits of applicability of the Hamiltonian, Eq. (12). We begin by seeking criteria of validity for the model. On the one hand, the consideration of quantum tunneling associated with a second level of energies is meaningful if $V_0 > E_1$, as evident from Fig. 1(a). If the eigenfunctions are approximated by the eigenfunctions of the harmonic oscillator, then this criterion can be approximated by $V_0 > (3/2)\hbar\omega$. Secondly, the diluteness condition given by Eq. (5) can be written in three dimensions as $N^{1/3}U_0^{3\mathrm{D}}/\Delta E \ll 1$ [25]. In 1D, this becomes

$$\frac{\omega N^{1/3} U_0^{3\mathrm{D}}}{\omega_\perp \Delta E} \ll 1 \tag{43}$$

which, contrary to the 3D case, accounts also for the geometrical compression in one of the dimensions through the term $\omega/\omega_\perp$. Here, it is also important to consider the restrictions on $\omega_\perp$ discussed at the beginning of Section 3. Finally, a last limit of the model is obtained when the coupling between levels is big enough to require more levels to characterize the eigenvectors. We obtain below the criterion delimiting when this coupling is too big. If this criterion is not fulfilled, more levels are required in the approximation or one should use the MCTDH method [32–34], depending on numerical efficiency requirements and spatial dimensionality. Other methods such as matrix product state algorithms, for example, time-evolving block decimation, can also of utility in this regime [51].

5.2 Discussion of the different regimes

The Josephson and Fock regimes are characterized by the criteria discussed above, Eqs. (29) and (30). Next we will show some numerical examples of the direct diagonalization of the Hamiltonian (12) for different sets of parameters, corresponding to different regimes. In Fig. 2 we show an example of the Josephson regime, $U_1 = U_0/2$, $U_{01} = (3/4)U_0$, $\zeta_0 = 10^2$, $J_1 = 5J_0$, $\Delta E = \sigma N U_0$, with $N = 10$ atoms and $\sigma = 2 \times 10^3$. In Fig. 2(a) we show all the Fock-space amplitudes $|c_i|^2$ for all the eigenvectors, while Fig. 2(b) shows a zoom of these for the lowest excited $3N + 3(N-1) + 1$ states. The first $N+1$ are eigenstates with no coupling to Fock vectors with atoms in the excited level. Then, the following $2N$ are eigenvectors where the Fock vectors show $N-1$ atoms in the lower level and one atom in the excited level. Finally, the following $3(N-1)$ show two atoms excited and $N-2$ in the lower level of eigenenergies (see Table 1). In Fig. 2(c) we show the Fock-space amplitudes $|c_i|^2$ for the ground state, $(N+1)$-th, and $(N+2)$-th excited eigenstates. These two figures show the HO behavior discussed in Section 4.2. In Fig. 2(d) we represent all the eigenvalues while in the inset in this figure we represent a zoom for the lowest excited $N+1$ eigenvectors, where the linear behavior described by Eq. (37) is shown. Every step in the values of the eigenvalues in Fig. 2(d) occurs when the corresponding eigenstate is the superposition of Fock vectors with one more atom occupying the second level

Table 1 Fock indices for the the Fock vectors up to the $(3N+3+3(N-1))$-th resulting from the ordering given in Eq. (26). These include all combinations with up to two particles excited.

Fock index i	N_0	N_1
1 to $N+1$	N	0
$N+2$ to $3N+2$	$N-1$	1
$3N+3$ to $3N+3+3(N-1)$	$N-2$	2

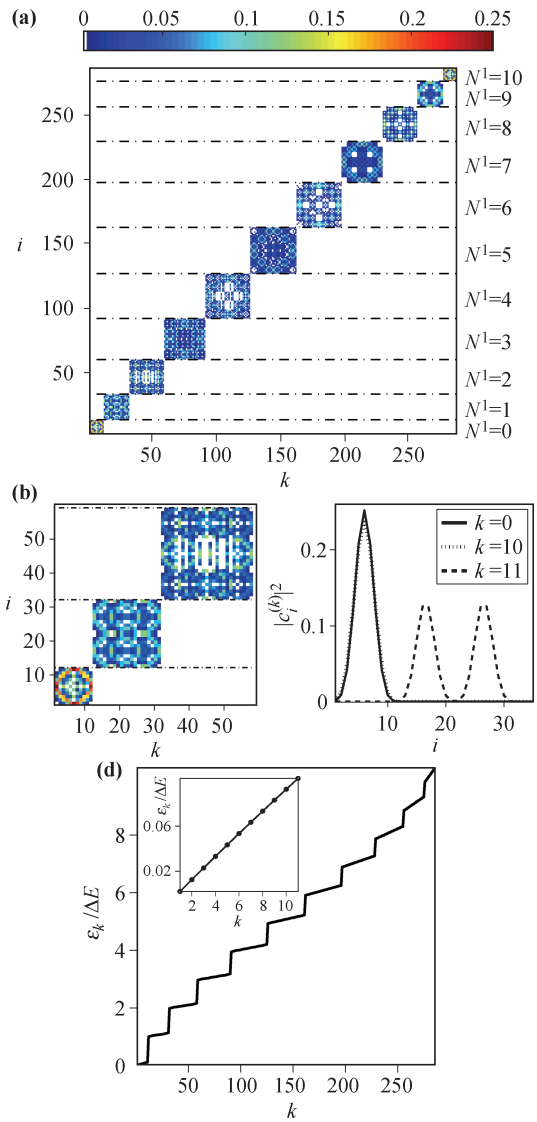

Fig. 2 Josephson regime example. **(a)** Fock-space amplitudes for all the eigenvectors, which show the harmonic oscillator behavior. **(b)** Zoom of panel (a). **(c)** Fock-space amplitudes for the ground state, $(N+1)$th, and $(N+2)$th excited eigenstates. **(d)** Eigenvalues as a function of Fock state index. *Inset*: lowest level approximation, first $N+1$ states only. The energy increases linearly, with characteristic jumps occurring each time a particle enters the excited level.

of energies. The increase in the slope in every step is due to the fact that $J_1 > J_0$. Indeed, for the last $N+1$ eigenvectors, for which all atoms are excited to the higher level, the slope is J_1.

If we reduce ζ_0 to one, we cannot assume that the parameters correspond clearly to the Fock or to the Josephson regime, as represented in Fig. 3(a). The Fock-space amplitudes $|c_i|^2$ of the $N+1$ lowest excited eigenvectors show different behavior for the ground state and for the $(N+1)$-th excited state, as represented in Figs. 3(b) and (c). The ground state is still an HO eigenstate, while the $(N+1)$-th excitation is a NOON-like state, as corresponding to the Fock regime. Figure 3(d) shows a different behavior than in the previous case. Particularly,

as shown in the inset in Fig. 3(d), the eigenvalues behave linearly for the five lowest excited eigenvectors. Then, the next six appear in quasidegenerate pairs with small splittings, as corresponds for the Fock regime. Notice that, since $J_1 > J_0$, the less excited $N+1$ eigenvectors behave as HO eigenstates. Then in this mixed regime, states with atoms occupying only the lower level can behave as in the Fock regime, while states with atoms occupying the excited level behave as in the Josephson one.

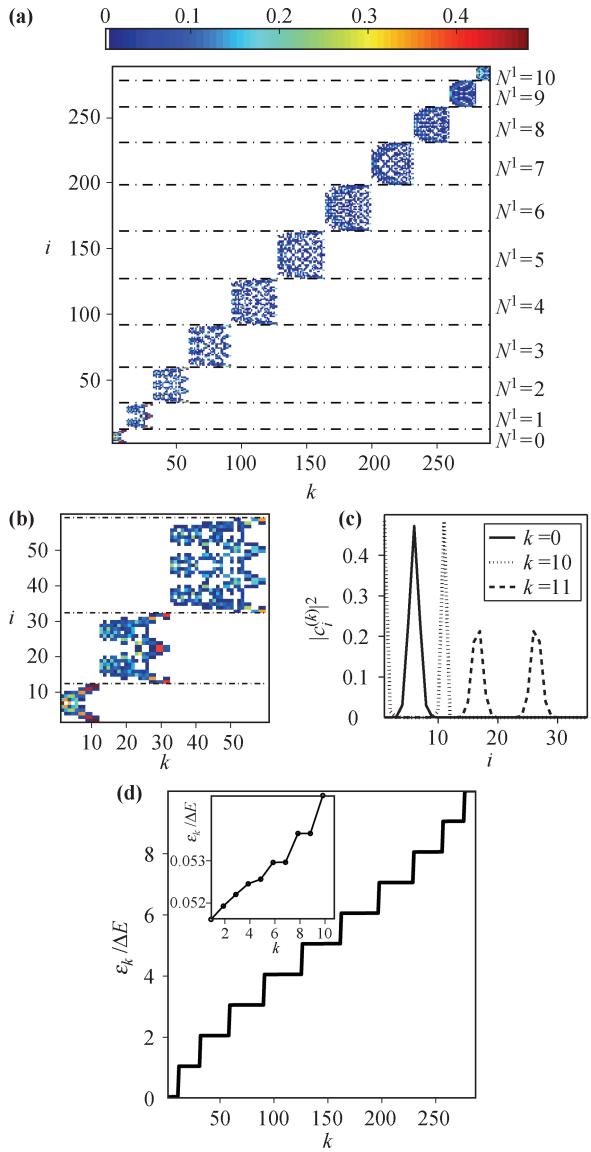

Fig. 3 Intermediate regime example. Panel layout as in Fig. 2. The lowest excited $N+1$ eigenvectors show no occupation of the lower level. Among these, the lowest excited 5 show harmonic oscillator behavior, while the next 6 eigenvectors behave as in the Fock regime. The eigenvalues show also this mixed HO–MS behavior. Notice that the $N+1$ more excited eigenstates of the spectra are harmonic oscillator like.

If we decrease ζ further, to $\zeta = 10^{-2}$, we enter clearly in the Fock regime, as represented in Fig. 4. Now, the eigenstates are MS states, as shown in Figs. 4(b) and (c), while the ground state is sharply peaked in $|N/2, N/2\rangle|0,0\rangle$. Also, Fig. 4(d) shows that the MS states appear in quasidegenerate symmetric/antisymmetric pairs, with small splittings in the eigenvalues (see also inset in this figure). Notice that, when atoms are excited, the presence of the term $2U_{01}\sum_{j,\ell\neq\ell'}\hat{n}_{j\ell}\hat{n}_{j\ell'}$ breaks the degeneracy in the $J_\ell = 0$ case between the vectors $|N_0-\nu,\nu\rangle|N_1-\nu',\nu'\rangle$ and $|N_0-\nu,\nu\rangle|\nu',N_1-\nu'\rangle$. For small J_ℓ, this in turn makes the MS states with $N_1 \neq 0$ appear also in pairs, and not as the superposition of four Fock vectors. These pairs can be observed in Fig. 4(b).

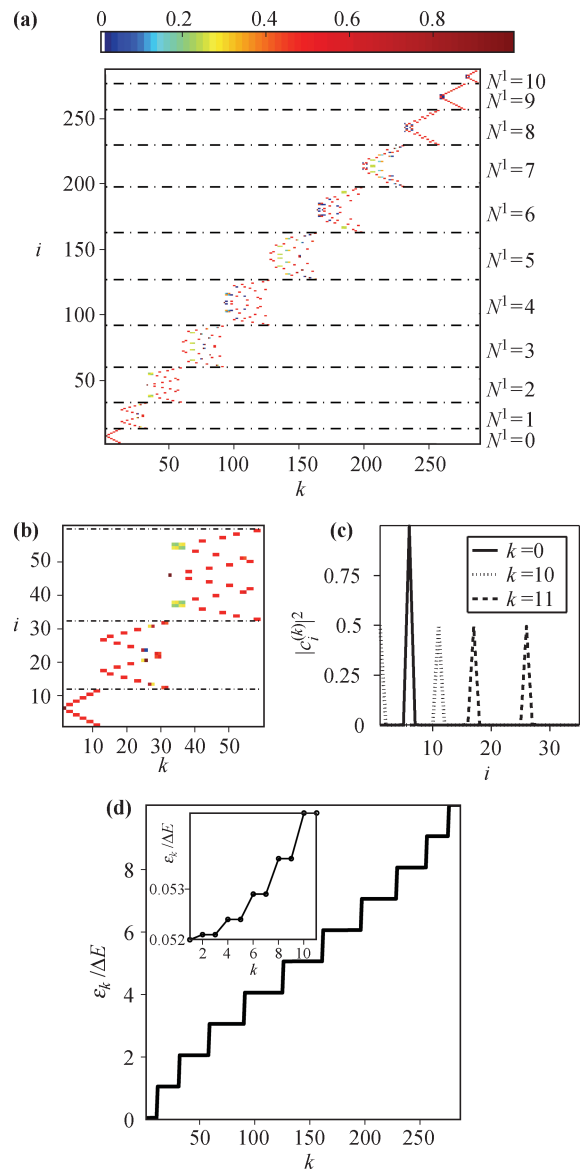

Fig. 4 A typical example in the Fock regime. Panel layout as in Fig. 2. Here, the eigenstates appear in quasidegenerate pairs of MS states.

Finally, the last regime is characterized by the presence of shadows of the MS states. Using perturbation theory we can show that the MS states $|n_{L,0}, n_{R,0}\rangle|0,0\rangle \pm |n_{R,0}, n_{L,0}\rangle|0,0\rangle$ couple to MS states showing two excited atoms $|n_{L,0}-2, n_{R,0}\rangle|2,0\rangle \pm |n_{R,0}, n_{L,0}-2\rangle|0,2\rangle$ and $|n_{L,0}, n_{R,0}-2\rangle|0,2\rangle \pm |n_{R,0}-2, n_{L,0}\rangle|2,0\rangle$ with coefficients

$$c_L = U_{01}\frac{\sqrt{2n_{L,0}(n_{L,0}-1)}}{U_0(6-4n_{L,0})+2U_1+2\Delta E}$$
$$c_R = U_{01}\frac{\sqrt{2n_{R,0}(n_{R,0}-1)}}{U_0(6-4n_{R,0})+2U_1+2\Delta E} \quad (44)$$

For the most excited MS state, $n_{L,0} = N$, and

$$c_N = U_{01}\frac{\sqrt{2N(N-1)}}{U_0(6-4N)+2U_1+2\Delta E} \quad (45)$$

If this coupling is not negligible, shadows of the MS states are coupled, and the upper level cannot be neglected, as discussed below.

5.3 Crossings of the eigenvalues

Let us show, for both regimes, bounds on the one- and two-level approximations other than criterion (45). With our choice of indexing states, the one-level approximation corresponds to truncating the size of the Hilbert space to $N+1$. With this definition of the one-level approximation, the bounds we present below will describe the regime in which this truncation is valid.

Let us consider first the crossings in the Josephson regime. The energy levels are coupled by the interaction energy U_{01}. Energy levels only become completely decoupled when $U_{01} = 0$. In this regime U_{01} is small, and then the coupling between levels is weak. Criterion (45) gives a good estimate of this coupling. Let us show that, although the energy levels are weakly coupled, eigenvalue crossings are induced by the presence of the excited level.

We consider first $U_0 = 0$, $U_1 = 0$ and $U_{01} = 0$. We find that the maximum of the eigenvalues for the first $N+1$ eigenstates with no occupation of the excited level coincides with the minimum of the eigenvalues of the states with one atom in the excited level if

$$\chi_{\rm Jos} = \frac{\triangle E}{J_0\,(2N-1)+J_1} = 1 \quad (46)$$

Equation (46), determines the first eigenvalue crossing in this regime. For $\chi_{\rm Jos} > 1$ no crossing occurs. In Fig. 5 we show an example where all the parameters are the same as in Fig. 2, that is $\zeta_0 = 10^2$, but with a smaller gap between levels, since $\sigma = 235$. As shown in Figs. 5(b) and (c) the $(N+1)$-th eigenvector shows occupation of the excited level. Notice that for small interactions, the presence of the excited level can induce this crossing. Figure 5(d) shows that the steps in the eigenvalues due to the excited atoms observed in Fig. 2(d) are now absent, since the excited atoms have now a much smaller energy. On the other hand, the inset in Fig. 5(d) shows that the behavior of the eigenvalues is still linear for all the eigenstates which are formed by superpositions of Fock vectors with the same number of excited atoms. For

$$\chi_{\rm Jos,gs} = \frac{\Delta E}{J_1 - J_0} = 1 \quad (47)$$

the first crossing involving the ground state occurs, i.e., the ground state is a state with non-zero occupation of the excited level if $\chi_{\rm Jos,gs} < 1$. This is, indeed, a limiting criterion for the validity of the model.

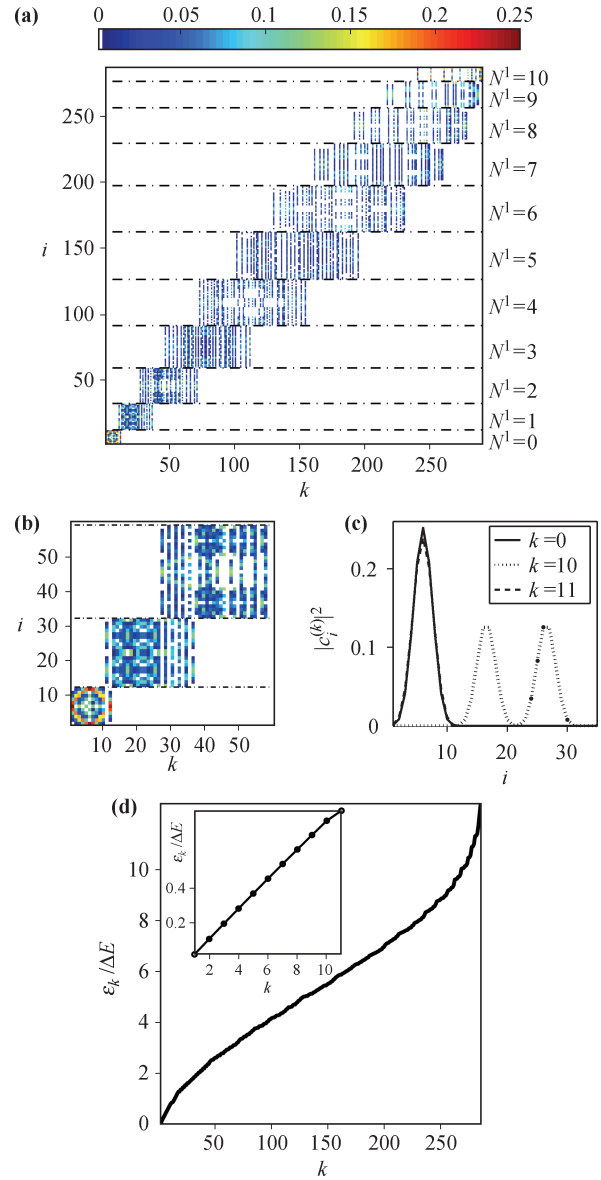

Fig. 5 First crossing in the Josephson regime. Panel layout as in Fig. 2. The first crossing in the Josephson regime is induced by the reduction of ΔE or increasing $J_1 - J_0$.

Analogously, in the Fock regime, the first eigenvalue crossings occurs when the condition

$$\chi_{\rm Fock} = \frac{\Delta E}{U_0(N^2/2+N-2)-2U_{01}(N/2-1)} = 1 \quad (48)$$

is met. This condition is obtained equating the maximum eigenvalue for states with no occupation of the excited level, to the minimum eigenvalue for states with one particle in the excited level. For $\chi_{\rm Fock} > 1$ no crossing takes place. In Fig. 6 we show an example for which all the parameters are the same as in Fig. 4, corresponding to the Fock regime, but now $\sigma = 5.35$. Here, the crossing appeared in the Fock regime, which can be due to the

reduction of the gap between levels or to the increasing of the interactions. Figure 5(d) and its inset show that the eigenvectors still appear as quasidegenerate symmetric/antisymmetric MS states, as discussed in Section 4.3.

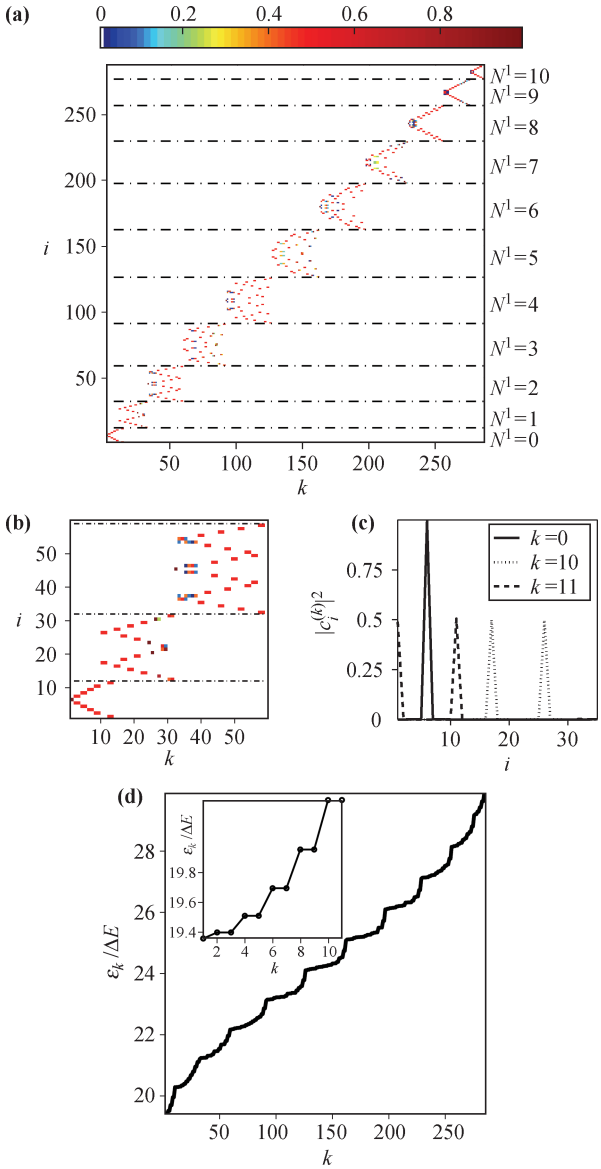

Fig. 6 First crossing in the Fock regime. Panel layout as in Fig. 2. The first crossing in this regime is induced by the reduction of ΔE or the increase in U_0.

If we increase further the interactions, or reduce the energy gap, shadows of the MS states appear, as discussed at the end of Section 5.2. For example, if we reduce the ΔE by taking $\sigma = 1.75$, the coupling between the MS states with no excited atoms and MS states with excited atoms is not negligible, as shown in Figs. 7(b) and (c).

Finally, the first crossing involving the ground state occurs when the condition

$$\chi_{\text{Fock,gs}} = \frac{\Delta E}{U_0(N-2) - 2U_{01}(N/2-1)} = 1 \qquad (49)$$

is satisfied. For $\chi_{\text{Fock,gs}} > 1$ the ground state shows non-zero occupation of the excited level. This criterion should be also considered as a limit for the validity of the model. As discussed in Section 5.1, when this limit is reached one must consider more energy levels or an MCTDH [32–34] or other many-body method [51].

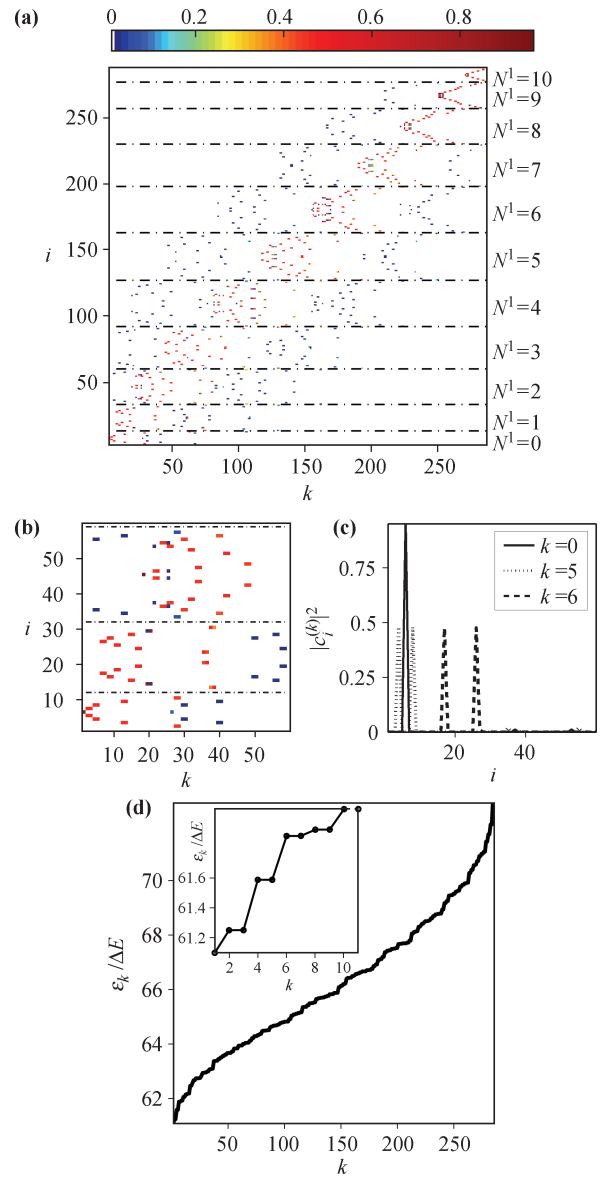

Fig. 7 Shadows of the MS states. Panel layout as in Fig. 2. If U_0 is increased, the MS states are coupled to Fock vectors with occupation of the excited level. The eigenvalues still behave as in the Fock regime.

In Fig. 8, the first $N + 1 + 2(N-1)$ eigenvalues are represented when ζ is reduced, for $\sigma = 100$. The eigenvectors behave as HO-like states for certain region, then as MS states, and finally, the most excited eigenstate with occupation only of the lower level crosses the least excited state with one atom excited when criterion (48) is reached. If ζ is increased further, shadows of the MS states appear, and eventually, the limit stated by criterion (49) is reached.

Therefore, the bounds to the one level approximation

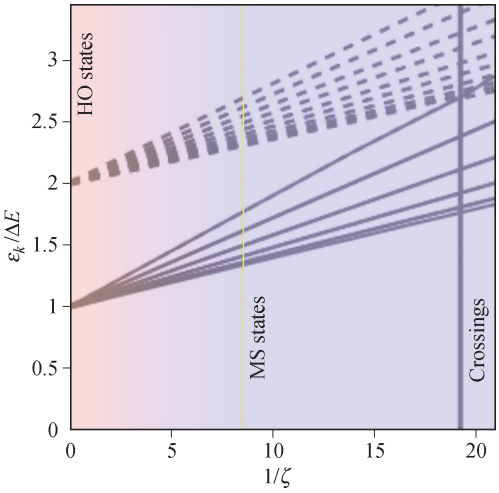

Fig. 8 Crossings as ζ is decreased. Shown are the eigenvalues of the $N+1$ eigenvectors with no occupation of the excited level (*solid line*) and the $2(N-1)$ eigenvalues of the eigenvectors showing only one excited atom. The ground state is non-degenerate, while the rest appear in quasidegenerate pairs. The dash-dotted line corresponds to the critical value of ζ at which the first crossing occurs, as calculated with (48). As ζ_0 is decreased, the eigenstates change from the Josephson regime, where they have are HO states, to the Fock regime, where they are MS states. If ζ is decreased further, crossings appear, and eventually, shadows of the MS states.

are given by criteria (46) and (48). We are interested in describing cat-like states which are typically excited eigenstates. Therefore, a characterization of eigenvalue crossings of energies other than the ground state are also relevant. These crossings appear when criteria (47) and (49) are satisfied.

6 Three-dimensional double well

The three dimensional (3D) double well was extensively studied in Ref. [25]. In this case $\omega \sim \omega_\perp$. The field operators in Hamiltonian (6) can be expanded in a fixed well localized single-particle basis obtained from the delocalized eigenfunctions of the single particle Hamiltonian $H_{\rm sp} = -\frac{\hbar^2}{2\mathcal{M}}\nabla^2 + V(\boldsymbol{x})$. These eigenfunctions are distortions of the eigenfunctions of the harmonic oscillator potential $V(\boldsymbol{x}) = \frac{1}{2}\omega^2\boldsymbol{x}^2$, given by

$$\psi_{n\ell m}(\boldsymbol{x}) \approx R_{n\ell}(r)Y_{\ell m}(\theta,\phi) \tag{50}$$

with $n \in \{0,1,2,\cdots\}$, $\ell \in \{n, n-2, n-4, \cdots, \ell_{\rm min}\}$, and $m \in \{-\ell,\ -\ell+1,\ \cdots,\ \ell-1,\ \ell\}$. Here $R_{n\ell}(r)$ is the radial part of the wavefunction, $Y_{\ell m}(\theta,\phi)$ are the familiar spherical harmonics, and $\ell_{\rm min}$ is 0 when n is even and 1 when n is odd. Then, n is the single-particle energy level, ℓ is the orbital angular momentum in 3D, and m is its z-projection. For the two level approximation $n = \ell$, and therefore the index n is superfluous and hereafter suppressed. These functions can be explicitly written in spherical coordinates for $\ell = 0, 1$ as

$$\psi_{00}(r,\theta,\varphi) = a_{\rm ho}^{-3/2}\pi^{-3/4}{\rm e}^{-r^2/(2a_{\rm ho}^2)}$$

$$\psi_{10}(r,\theta,\varphi) = a_{\rm ho}^{-3/2}\sqrt{2}\pi^{-3/4}(r/a_{\rm ho}){\rm e}^{-r^2/(2a_{\rm ho}^2)}\cos\theta$$

$$\psi_{1\pm1}(r,\theta,\varphi) = a_{\rm ho}^{-3/2}\pi^{-3/4}(r/a_{\rm ho}){\rm e}^{-r^2/(2a_{\rm ho}^2)}\sin\theta{\rm e}^{\pm{\rm i}\varphi}$$

The energy of an atom associated with the wavefunction $\psi_{\ell m}(\boldsymbol{x}-\boldsymbol{x}_j)$ is

$$E_n \approx \hbar\omega\left(n+\frac{3}{2}\right) \tag{51}$$

In general, the spherical harmonics cannot be accurately used as a basis. In particular, they give poor approximations of the overlap between functions localized in different wells. Then, the localized functions at well j can be obtained numerically as

$$\psi_{j00}(\boldsymbol{x}) = \phi(x)^0\phi(y)^0\psi_{j0}(z) \tag{52}$$

$$\psi_{j10}(\boldsymbol{x}) = \phi(x)^0\phi(y)^0\psi_{j1}(z) \tag{53}$$

$$\psi_{j,1\pm1}(r,\theta,\varphi)(\boldsymbol{x}) = \frac{1}{\sqrt{2}}\left[\phi^1(x)\phi^0(y)\psi_{j0}(z) \pm {\rm i}\phi^0(x)\phi^1(y)\psi_{j0}(z)\right] \tag{54}$$

where $\phi^\ell(x)$ and $\phi^\ell(y)$ are two lowest excited eigenfunctions of the harmonic oscillator in the x and y directions, and $\psi_{j\ell}(z)$ are the on-well localized eigenfunctions of the double well given in Eqs. (10) and (11), respectively. The four modes localized in one of the wells are represented schematically in Fig. 1(b).

Then, we can expand the field operator in Eq. (1) in terms of this eight mode basis as

$$\hat{\Psi}(\boldsymbol{x}) = \sum_{j,\ell,m}\hat{b}_{j\ell m}\psi_{\ell m}(\boldsymbol{x}-\boldsymbol{x}_j) \tag{55}$$

where $\boldsymbol{x}_1 \equiv -\boldsymbol{x}_{\rm min}$ and $\boldsymbol{x}_2 \equiv \boldsymbol{x}_{\rm min}$ are the minima of the left and right wells. The operators $\hat{b}^\dagger_{j\ell m}$ and $\hat{b}_{j\ell m}$ satisfy the usual bosonic annihilation and creation commutation relations,

$$[\hat{b}_{j\ell m},\ \hat{b}^\dagger_{j'\ell'm'}] = \delta_{jj'}\delta_{\ell\ell'}\delta_{mm'}$$
$$[\hat{b}^\dagger_{j\ell m},\ \hat{b}^\dagger_{j'\ell'm'}] = [\hat{b}_{j\ell m},\ \hat{b}_{j'\ell'm'}] = 0 \tag{56}$$

By using this eight-mode expansion of the field operator, the 3D Hamiltonian was obtained:

$$\hat{H} = \sum_{\ell,m}\hat{H}_{\ell m} + \hat{H}_{\rm int} \tag{57}$$

The first term is a sum over LMGHs for each level, similar to the one discussed in Section 3 [see Eq. (13)]:

$$H_{\ell m} = U_{\ell m}\sum_j\hat{n}_{j\ell m}(\hat{n}_{j\ell m}-1) - J_{\ell m}\sum_{j'\neq j}\hat{b}^\dagger_{j\ell m}\hat{b}_{j'\ell m} + E_\ell\sum_j\hat{n}_{j\ell m} \tag{58}$$

In Eq. (58), the term $E_\ell\sum_j\hat{n}_{j\ell m}$ accounts for the energy of the atoms at level ℓ and z component of angular momentum m, with $\hat{n}_{j\ell m} = \hat{b}^\dagger_{j\ell m}\hat{b}_{j\ell m}$ the number operator. The term

$$\hat{H}_{\rm int} = \sum_m \hat{H}^m_{\rm inter} + \hat{H}_{\rm intra} \tag{59}$$

accounts for processes among atoms in different levels and with different z component of the angular momentum.

There are three relevant processes in Eq. (59). The first of these is given by

$$\hat{H}^0_{\rm inter} = \sum_j \Big\{ U^{00}_{01} \left[\left(\hat{b}^\dagger_{j00}\right)^2 \left(\hat{b}_{j10}\right)^2 + h.c. \right] + 4\, U^{00}_{01}\, \hat{n}_{j00}\, \hat{n}_{j10} \Big\} \tag{60}$$

This process describes the excitation of two atoms from the ground state to an orbital with $m = 0$, or conversely, their decay from an excited state with $m = 0$ to the ground state. We name this process *zero-vorticity interlevel hopping*. The second is

$$\hat{H}^1_{\rm inter} = \sum_j \Big\{ U^{01}_{01} \left[\left(\hat{b}^\dagger_{j00}\right)^2 \hat{b}_{j11} \hat{b}_{j1,-1} + h.c. \right] + 4\, U^{01}_{01} \left(\hat{n}_{j00} \left(\hat{n}_{j11} + \hat{n}_{j1,-1} \right) \right) \Big\} \tag{61}$$

This process is similar to the first one and we call it *vortex–antivortex interlevel hopping*. It permits an atom to change its level and also its z component of its angular momentum, m. Through this process two atoms in the ground state can be excited, one with $m = 1$ (a vortex) and the other with $m = -1$ (an anti-vortex). Conversely, one atom with $m = +1$ and another with $m = -1$ can decay to the ground state. Finally, the third process is

$$\hat{H}_{\rm intra} = \sum_j \Big\{ U^{01}_{11} \left[\left(\hat{b}^\dagger_{j10}\right)^2 \hat{b}_{j11} \hat{b}_{j1,-1} + h.c. \right] + 2\, U^{01}_{11} \left(\hat{n}_{j10} \left(\hat{n}_{j11} + \hat{n}_{j1,-1} \right) + 2\, U_{11} \left(\hat{n}_{j11} \hat{n}_{j1,-1} \right) \right) \Big\} \tag{62}$$

Through the third process, *vortex–antivortex intralevel hopping*, the atoms can only change their angular properties, but not their energy level. Then, two excited atoms with $m = 0$ can generate a pair of atoms, one with $m = 1$ and the other with $m = -1$ or vice versa. These three processes are represented schematically in Fig. 1(b). Again, in obtaining this Hamiltonian, the off-site interaction coefficients were neglected, as discussed in Section 3 for the 1D case.

Notice that the 3D interaction and tunneling coefficients that appear in the LMGH part of this Hamiltonian, Eq. (58), have to be evaluated independently for atoms in the same level and with the same m. The tunneling coefficients in Eq. (58) are defined as

$$J_{\ell m} = -\int {\rm d}^3\boldsymbol{x} \psi^*_{\ell m}(\boldsymbol{x} - \boldsymbol{x}_{\rm min}) \left[-\frac{\hbar^2}{2\mathcal{M}} \nabla^2 + V(\boldsymbol{x}) \right] \times \psi_{\ell m}(\boldsymbol{x} + \boldsymbol{x}_{\rm min}) \tag{63}$$

The interaction coefficients are

$$U^{\ell' m'}_{\ell m} = \frac{g}{2} \int {\rm d}^3\boldsymbol{x} |\psi_{\ell m}(\boldsymbol{x})|^2 |\psi_{\ell' m'}(\boldsymbol{x})|^2 \tag{64}$$

Notice that the coefficients in the coupling part of the Hamiltonian, Eqs. (60)–(62), are related to the interaction coefficients, and not to tunneling coefficients.

The presence of many new coefficients makes necessary a wider characterization of regimes, further away from the 1D Josephson, intermediate, and Fock regimes (where the eigenvectors and eigenvalues behave as in Figs. 2, 3, and 4). This was accomplished in [25], where criteria for the crossings and limits of the model were also given, and represented numerically for the particular case of the Duffing double well potential $V(z) = V_0(-8z^2/a^2 + 16z^4/a^4 + 1)$. A Josephson and Fock regime can be described, for which the eigenvectors can be characterized as HO-like or MS states, respectively. These MS states can show occupation of the excited level, resulting in an MS of angular degrees of freedom. The presence of these orbitals are the fundamental difference from the 1D case. Moreover, the three coupling processes described above give rise to interesting dynamical phenomena, like vortex tunneling and vortex/antivortex creation/annihilation along with the tunneling of atoms with non-zero m. These new dynamical phenomena are the subject of our upcoming work [52].

7 Conclusions

Ultracold bosons in double well potentials are a simple system to study a great variety of physical phenomena. There are two main processes: the atoms can interact in pairs on-well with energy U_0 or tunnel to the other well with energy J_0. When the interactions dominate over the tunneling energies in the system, the spectra of the eigenvectors are characterized by the presence of MS states. But also in this case it is necessary to consider the possibility that the atoms populate an excited level. Then, other energies are relevant, including the interaction energy of the atoms in the excited level U_1, the tunneling energy in the excited level J_1, and the single-particle energy gap between levels, ΔE.

In this article, we used a two level approach to describe the possible physical scenarios in one- and three-dimensional double wells. For the 1D case, we clearly identified the Josephson regime, for which quantum tunneling was experimentally demonstrated. We characterized the eigenvectors and eigenvalues in the noninteracting regime, and we showed through direct diagonalization of the two level LMGH that this behavior can be extended to the Josephson regime. Our interest was mainly in the occurrence of MS states of atoms localized in either one or the other well, which appear for bigger interactions, in the Fock regime. We characterized the appearance of crossings in the spectra, which serves

as a limiting criterion for the validity of the one-level or LMGH approximation. We obtained also the limits of the two-level approximation. In particular, we found when the interactions are sufficiently large that coupling to states with non-zero occupation of the excited level is relevant. In this case, the interaction coefficient can overcome the energy gap between levels, and then the states show non-zero occupation of the excited level. We described numerically the transition from the Josephson regime to the Fock regime. We introduced a new Josephson–Fock *mixed regime*, in which the most excited eigenvectors with no occupation of the excited level behave as MS states while the less excited ones are HO-like states. Moreover, since $J_1 \gg J_0$, when the eigenvectors involve only atoms in the excited level, they behave as HO-like states.

MS states are, unfortunately, highly excited states and fragile against decoherence processes [40, 53]. Thus they are difficult to observe experimentally. Quantum superpositions of matter waves have been observed for few particles, like electrons, but remains a challenging problem for larger objects; experiments with C_{60} molecules are in the lead at present in such efforts (see Refs. [54, 55], and references therein), but ultracold bosons have the potential to go to hundreds or thousands of particles in an MS state. Therefore, there are many theoretical proposals for realizing them in a BEC experiment [17, 37, 56–66], and this remains an appealing research topic with deep physical implications. The two-level scenario introduces the possibility to study other initial states with non-zero occupation of the excited level, which could be the key to realize MS states experimentally, as discussed in Ref. [37]. Also, the two-level approach in three dimensions permits one to consider angular degrees of freedom in the problem [25]. The angular degrees of freedom are a very interesting topic in systems of ultracold atoms in optical lattices [67–72], where the excitation of part of the population to a p level was demonstrated experimentally [73, 74]. Here, we summarized the derivation of the Hamiltonian and the MS states. Then, the study of the dynamics of ultracold atoms in three dimensional double wells where orbital degrees of freedom play a relevant role is an interesting topic for future research.

Acknowledgements This material is based in part upon work supported by the National Science Foundation under grant numbers PHY-0547845 and PHY-1067973. L. D. Carr thanks the Alexander von Humboldt foundation and the Center for Quantum Dynamics for additional support. M. A. Garcia-March acknowledges the Fulbright Foundation, FECYT, and the Spanish Ministry of Education and Science.

References

1. A. J. Leggett, J. Phys.: Condens. Matter, 2002, 14(15): R415
2. D. R. Dounas-Frazer, A. M. Hermundstad, and L. D. Carr, Phys. Rev. Lett., 2007, 99(20): 200402
3. G. Mazzarella, L. Salasnich, A. Parola, and F. Toigo, Phys. Rev. A, 2011, 83(5): 053607
4. X. X. Yang and Y. Wu, Commun. Theor. Phys., 2009, 52: 244
5. A. J. Leggett, Rev. Mod. Phys., 2001, 73(2): 307
6. F. Dalfovo, S. Giorgini, L. P. Pitaevskii, and S. Stringari, Rev. Mod. Phys., 1999, 71(3): 463
7. J. Javanainen, Phys. Rev. Lett., 1986, 57(25): 3164
8. G. J. Milburn, J. Corney, E. M. Wright, and D. F. Walls, Phys. Rev. A, 1997, 55(6): 4318
9. A. Smerzi, S. Fantoni, S. Giovanazzi, and S. R. Shenoy, Phys. Rev. Lett., 1997, 79(25): 4950
10. I. Zapata, F. Sols, and A. J. Leggett, Phys. Rev. A, 1998, 57(1): R28
11. E. A. Ostrovskaya, Y. S. Kivshar, M. Lisak, B. Hall, F. Cattani, and D. Anderson, Phys. Rev. A, 2000, 61(3): 031601
12. C. Lee, W. Hai, X. Luo, L. Shi, and K. Gao, Phys. Rev. A, 2003, 68(5): 053614
13. C. Lee, W. Hai, L. Shi, and K. Gao, Phys. Rev. A, 2004, 69(3): 033611
14. D. Ananikian and T. Bergeman, Phys. Rev. A, 2006, 73(1): 013604
15. G. F. Wang, L. B. Fu, and J. Liu, Phys. Rev. A, 2006, 73(1): 013619
16. W. D. Li and J. Liu, Phys. Rev. A, 2006, 74(6): 063613
17. K. W. Mahmud, H. Perry, and W. P. Reinhardt, Phys. Rev. A, 2005, 71(2): 023615
18. B. Julia-Diaz, J. Martorell, M. Mele-Messeguer, and A. Polls, Phys. Rev. A, 2010, 82(6): 063626
19. M. Albiez, R. Gati, J. Fölling, S. Hunsmann, M. Cristiani, and M. K. Oberthaler, Phys. Rev. Lett., 2005, 95(1): 010402
20. S. Giovanazzi, A. Smerzi, and S. Fantoni, Phys. Rev. Lett., 2000, 84(20): 4521
21. S. Levy, E. Lahoud, I. Shomroni, and J. Steinhauer, Nature, 2007, 449(7162): 579
22. M. J. Steel and M. J. Collett, Phys. Rev. A, 1998, 57(4): 2920
23. S. G. Kalosakas and A. R. Bishop, Phys. Rev. A, 2002, 65(4): 043616
24. C. Lee, Phys. Rev. Lett., 2006, 97(15): 150402
25. M. A. Garcia-March, D. R. Dounas-Frazer, and L. D. Carr, Phys. Rev. A, 2011, 83(4): 043612
26. H. J. Lipkin and A. J. Glick, Nucl. Phys., 1965, 62(2): 188
27. J. Vidal, G. Palacios, and C. Aslangul, Phys. Rev. A, 2004, 70(6): 062304
28. D. R. Dounas-Frazer, *et al.*, Master's Thesis, 2007
29. B. Wu and Q. Niu, Phys. Rev. A, 2000, 61(2): 023402
30. J. Liu, L. Fu, B. Y. Ou, S. G. Chen, D. I. Choi, B. Wu, and Q. Niu, Phys. Rev. A, 2002, 66(2): 023404
31. B. Wu and J. Liu, Phys. Rev. Lett., 2006, 96(2): 020405
32. D. Masiello, S. B. McKagan, and W. P. Reinhardt, Phys. Rev. A, 2005, 72(6): 063624
33. A. I. Streltsov, O. E. Alon, and L. S. Cederbaum, Phys. Rev. A, 2006, 73(6): 063626
34. O. E. Alon, A. I. Streltsov, and L. S. Cederbaum, Phys. Rev. A, 2008, 77(3): 033613

35. S. Zollner, H. D. Meyer, and P. Schmelcher, Phys. Rev. A, 2008, 78(1): 013621
36. K. Sakmann, A. I. Streltsov, O. E. Alon, and L. S. Cederbaum, Phys. Rev. Lett., 2009, 103(22): 220601
37. L. D. Carr, D. R. Dounas-Frazer, and M. A. Garcia-March, Europhys. Lett., 2010, 90(1): 10005
38. S. Dusuel, J. Vidal, J. M. Arias, J. Dukelsky, and J. E. Garcia-Ramos, Phys. Rev. C, 2005, 72(6): 064332
39. J. I. Cirac, M. Lewenstein, K. Molmer, and P. Zoller, Phys. Rev. A, 1998, 57(2): 1208
40. D. A. R. Dalvit, J. Dziarmaga, and W. H. Zurek, Phys. Rev. A, 2000, 62(1): 013607
41. T. Schumm, S. Hofferberth, L. M. Andersson, S. Wildermuth, S. Groth, I. Bar-Joseph, J. Schmiedmayer, and P. Krüger, Nat. Phys., 2005, 1: 57
42. B. V. Hall, S. Whitlock, R. Anderson, P. Hannaford, and A. I. Sidorov, Phys. Rev. Lett., 2007, 98(3): 030402
43. R. Gati, J. Esteve, B. Hemmerling, T. B. Ottenstein, J. Appmeier, A. Weller, and M. K. Oberthaller, New J. Phys., 2006, 8(9): 189
44. F. W. Strauch, M. Edwards, E. Tiesinga, C. Williams, and C. W. Clark, Phys. Rev. A, 2008, 77(5): 050304(R)
45. J. Sebby-Strabley, M. Anderlini, P. S. Jessen, and J. V. Porto, Phys. Rev. A, 2006, 73(3): 033605
46. T. Calarco, U. Dorner, P. S. Julienne, C. J. Williams, and P. Zoller, Phys. Rev. A, 2004, 70(1): 012306
47. M. Olshanii, Phys. Rev. Lett., 1998, 81(5): 938
48. Z. Idziaszek and T. Calarco, Phys. Rev. A, 2006, 74(2): 022712
49. N. W. Ashcroft and N. D. Mermin, Solid State Physics, Holt: Rinehart and Winston, 1976
50. R. W. Spekkens and J. E. Sipe, Phys. Rev. A, 1999, 59(5): 3868
51. U. Schollwoeck, Ann. Phys., 2011, 326: 96
52. M. A. Garcia-March and L. D. Carr, In preparation
53. H. Pichler, A. J. Daley, and P. Zoller, Phys. Rev. A, 2010, 82(6): 063605
54. M. Arndt, O. Nairz, J. Vos-Andreae, C. Keller, G. van der Zouw, and A. Zeilinger, Nature, 1999, 401(6754): 680
55. B. Brezger, L. Hackermüller, S. Uttenthaler, J. Petschinka, M. Arndt, and A. Zeilinger, Phys. Rev. Lett., 2002, 88(10): 100404
56. C. Menotti, J. R. Anglin, J. I. Cirac, and P. Zoller, Phys. Rev. A, 2001, 63(2): 023601
57. J. Higbie and D. M. Stamper-Kurn, Phys. Rev. A, 2004, 69(5): 053605
58. Y. P. Huang and M. G. Moore, Phys. Rev. A, 2006, 73(2): 023606
59. J. A. Dunningham, K. Burnett, R. Roth, and W. D. Phillips, New J. Phys., 2006, 8(9): 182
60. F. Piazza, L. Pezze, and A. Smerzi, Phys. Rev. A, 2008, 78(5): 051601(R)
61. G. Ferrini, A. Minguzzi, and F. W. J. Hekking, Phys. Rev. A, 2008, 78(2): 023606
62. I. E. Mazets, G. Kurizki, M. K. Oberthaler, and J. Schmiedmayer, Europhys. Lett., 2008, 83(6): 60004
63. G. Watanabe, Phys. Rev. A, 2010, 81(2): 021604(R)
64. Z. F. Xu, P. Zhang, R. Lu, and L. You, Phys. Rev. A, 2010, 81(5): 053619
65. D. W. Hallwood, T. Ernst, and J. Brand, Phys. Rev. A, 2010, 82(6): 063623
66. R. Kanamoto and E. M. Wright, J. Opt., 2011, 13(6): 064011
67. M. Lewenstein and W. V. Liu, Nat. Phys., 2011, 7(2): 101
68. A. Isacsson and S. M. Girvin, Phys. Rev. A, 2005, 72(5): 053604
69. V. W. Scarola and S. Das Sarma, Phys. Rev. Lett., 2005, 95(3): 033003
70. W. V. Liu and C. Wu, Phys. Rev. A, 2006, 74(1): 013607
71. C. Xu and M. P. A. Fisher, Phys. Rev. B, 2007, 75(10): 104428
72. A. Collin, J. Larson, and J. P. Martikainen, Phys. Rev. A, 2010, 81(2): 023605
73. T. Müller, S. Fölling, A. Widera, and I. Bloch, Phys. Rev. Lett., 2007, 99(20): 200405
74. G. Wirth, M. Ölschläger, and A. Hemmerich, Nat. Phys., 2011, 7(2): 147